Stabilization of oxidized Cu species via CeO_x nano-islands for enhanced CO_2 reduction to C_{2+} products

Miaojin Wei[1,†], Jiawei Li[1,2,†], Jiankang Zhao[1], Sunpei Hu[1], Yuan Ji[2], Weiqing Xue[1], Yizhou Dai[1], Haoyuan Wang[1], Xinyan Zhang[1], Kwun Nam Hui[3], Xu Li[2], Chuan Xia[2], Tingting Zheng[2] and Jie Zeng[1,4,*]

[1]Hefei National Research Center for Physical Sciences at the Microscale, Key Laboratory of Strongly-Coupled Quantum Matter Physics of Chinese Academy of Sciences, Key Laboratory of Surface and Interface Chemistry and Energy Catalysis of Anhui Higher Education Institutes, Department of Chemical Physics, University of Science and Technology of China, Hefei 230026, China

[2]School of Materials and Energy, University of Electronic Science and Technology of China, Chengdu 611731, China

[3]Joint Key Laboratory of the Ministry of Education, Institute of Applied Physics and Materials Engineering, University of Macau, Avenida da Universidade, Taipa, Macau SAR, China

[4]School of Chemistry & Chemical Engineering, Anhui University of Technology, Ma'anshan 243002, China

*Corresponding author. E-mail: zengj@ustc.edu.cn

[†]Equally contributed to this work.

ABSTRACT

The presence of oxidized copper species (CuO_x) on metallic Cu surfaces is widely acknowledged as a critical factor for promoting C–C coupling during CO_2 reduction reactions (CO_2RR). However, the inherent instability of CuO_x under negative potentials, where it is prone to reduction to metallic Cu, remains a formidable challenge. In this study, we developed a CeO_x-modified CuO catalyst for the CO_2RR, featuring CeO_x uniformly distributed as isolated nano-islands on CuO nanoparticles. Upon reduction of the CuO matrix to metallic Cu, the CeO_x layer effectively stabilizes the interfacial CuO_x, preventing its further reduction. *Operando* characterization verified the sustained presence of Cu^{2+} and Cu^{+} species at highly reductive potentials, underscoring the role of CeO_x in preserving CuO_x stability. Theoretical calculations revealed that Ce^{3+} enhances the formation energy of oxygen vacancies, stabilizing the CuO_x interface and *OC–CO intermediates, which are crucial for C–C coupling. With this surface modification strategy, the catalyst achieved a remarkable C_{2+} faradaic efficiency of 78% at −700 mA cm^{-2}, while demonstrating persistent performance with a faradaic efficiency exceeding 70% for C_{2+} products at −100 mA cm^{-2} for over 110 hours. These findings present an effective strategy for stabilizing metal oxides and advancing durable CO_2RR catalysts.

Keywords: CO_2 reduction reaction, C_{2+} products, oxidized copper stabilization, CeO_x nano-islands, C–C coupling efficiency.

INTRODUCTION

The rising concentration of CO_2 in the atmosphere has led to the search for effective strategies to utilize this abundant greenhouse gas [1]. CO_2 reduction reactions (CO_2RR), driven by renewable energy, offer a promising pathway for converting CO_2 into valuable chemical products, enabling a closed-loop carbon economy [2]. Among the diverse products, C_{2+} compounds such as ethylene, ethanol, and acetate are particularly attractive due to their higher economic value compared to C_1 products [3–5]. Copper (Cu)-based catalysts are widely regarded as the most effective for facilitating C_{2+} product formation in the CO_2RR, which is attributed to their moderate adsorption of key intermediates [6]. However, achieving high selectivity and activity for C_{2+} products remains challenging and requires precise manipulation of the reaction pathways and catalyst properties.

The efficiency of C_{2+} production is closely linked to the C–C coupling, where *CO and *CO (or *CHO) intermediates interact to form $*C_2$ species [7]. One effective strategy to improve C–C coupling is to increase the surface coverage of *CO and other key intermediates [8–14]. It has been observed that copper in higher oxidation states, such as Cu^+/Cu^{2+}, exhibits stronger CO adsorption and lower activation barriers for C–C coupling than metallic Cu does, making it a promising candidate for promoting higher-order carbon product formation [15–20]. As such, stabilizing CuO_x species on Cu surfaces is essential for improving C_{2+} faradaic efficiency (FE) [21,22]. However, maintaining CuO_x at the reductive potential during the CO_2RR is challenging, as CuO_x is prone to reduction to metallic Cu under reducing conditions [23,24].

Efforts to stabilize CuO_x species have led to the development of several strategies [26,27]. One approach involves the synthesis of copper salts, such as $Cu_3(PO_4)_2$, which are relatively stable and resistant to reduction [28]. While this method has yielded a high C_{2+} FE of ~90%, the stability remains limited due to the gradual reduction of Cu^{2+} to Cu^0, with operational lifetimes of less than 20 hours. Another promising strategy is the modification of Cu with transition metal oxides (MO_x), which can effectively preserve CuO_x species and promote efficient C–C coupling at the CuO_x/Cu interface [29–33]. Studies have explored the dispersion of Cu onto bulk MO_x supports or the uniform mixing of Cu and MO_x nanoparticles to maximize the interface density [34–39]. However, these configurations often compromise conductivity due to the spatial separation of Cu particles, which hinders electron transport and reduces catalytic efficiency. Therefore, achieving an optimal Cu-MO_x configuration requires delicate design to balance

conductivity and stability, thereby increasing C_{2+} efficiency [40–42].

Here, we present a CeO_x modified Cu catalyst (CeO_x/CuO), where CeO_x was dispersed as nano-islands on the Cu surface, enabling efficient CO_2 reduction to C_{2+} products. *Operando* studies revealed that under a negative potential, bulk CuO was completely reduced to metallic Cu, whereas Cu modified with CeO_x nano-islands retained its oxidation state. The CeO_x/CuO catalyst, with its optimized CuO_x/Cu interface, exhibited a high C_{2+} FE of 78% at a partial current density of −545 mA cm^{-2}. Additionally, the CeO_x/CuO catalyst demonstrated high stability, maintaining over 70% C_{2+} FE at a current density of −100 mA cm^{-2} for 110 hours. Theoretical calculations supported the proposed mechanism, showing that CeO_x facilitates the preservation of CuO_x species, which in turn stabilize *OC–CO intermediates and enhance C–C coupling by lowering the reaction barriers.

RESULTS AND DISCUSSION

Stabilizing CuO_x under reductive conditions of the CO_2RR is difficult because of the thermodynamic tendency of oxidized copper species to reduce to metallic Cu. As shown in Fig. 1a, the standard reduction potentials of $Cu(OH)_2$ to Cu (+0.61 V *vs*. Reversible Hydrogen Electrode, RHE) and Cu_2O to Cu (+0.47 V *vs*. RHE) reveal their strong propensity for reduction at typical CO_2RR operating potentials (~−0.9 V *vs*. RHE). This reduction undermines the stability of high-valence-state Cu, which is critical for facilitating C_{2+} product formation. To address this limitation, efforts have been directed toward stabilizing CuO_x species by incorporating metal oxides (MO_x) during the CO_2RR. Fig. 1b illustrates that CuO_x forms at the interface between bulk Cu and bulk MO_x, but the interfacial area between Cu and MO_x is limited. One approach to increase the interfacial area, as shown in Fig. 1c, involves dispersing Cu particles onto bulk MO_x supports. However, this configuration often suffers from poor conductivity due to the insulating nature of bulk MO_x. An alternative strategy, depicted in Fig. 1d, employs a uniform mixture of Cu and MO_x nanoparticles to maximize the interface density. While this design enhances the interfacial area, it compromises the conductivity because of the spatial separation of the Cu particles. To overcome the trade-off between the interface density and conductivity, a more effective strategy is proposed in Fig. 1e, where ultra-small MO_x nanoparticles are uniformly dispersed onto bulk Cu. This configuration ensures a high density of active interfaces while maintaining good conductivity, ultimately enhancing both the catalytic

activity and stability. In addition to optimizing the Cu-MO_x interface, selecting a metal oxide with low solubility and reduced reducibility is essential for achieving long-term stability under the reductive conditions of the CO_2RR. Ce oxides were chosen for this study because of their inherently low solubility and reduced reducibility compared with those of other metal oxides, making them ideal candidates for stabilizing CuO_x species.

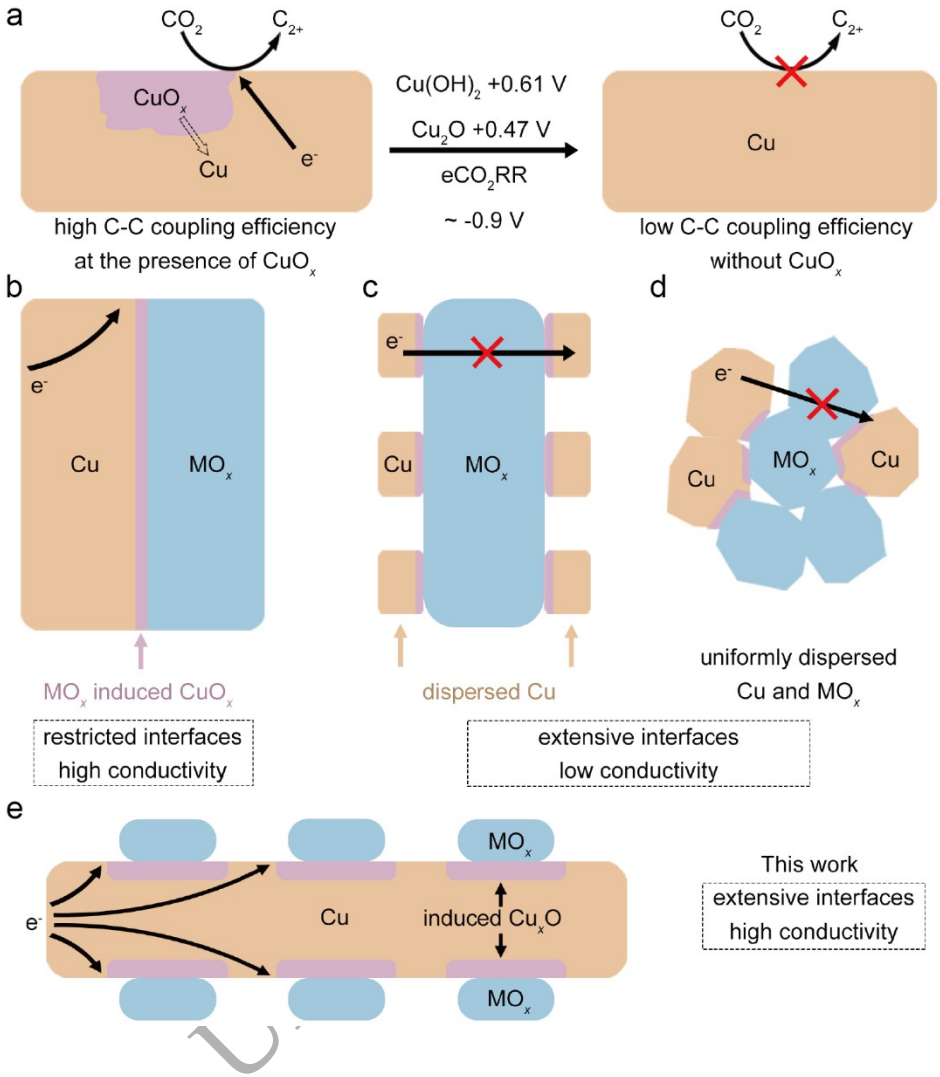

Figure 1 (a) CuO_x (purple area) promotes the formation of C_{2+} products, but it is easily reduced into metallic Cu and thus decreases C_{2+} production. (b) CuO_x forms at the interface of Cu and MO_x. However, the interface between bulk MO_x and bulk Cu is restricted. When Cu is dispersed on (c) bulk MO_x and (d) dispersed MO_x, the interface is extensive, but these assemblies suffer from the poor conductivity of bulk MO_x. (e) MO_x is reversely dispersed on Cu, which optimizes the balance between the interface density and conductivity.

Following the identification of the optimal configuration, we explored the synthesis of Cu catalysts modified with CeO_x species. The CeO_x/CuO catalyst was synthesized using a strong

electrostatic adsorption method (Fig. 2a) [43]. First, CuO nanoparticles are synthesized via the calcination of CuC_2O_4 at 623 K in air, and then 20–50 nm CuO nanoparticles are obtained (Fig. S1). For the deposition of CeO_x, $Ce(NO_3)_3$ was dissolved in a suspension of CuO nanoparticles, and the pH of the solution was adjusted by adding KOH to exceed the point of zero charge (pzc ~7.6) of CuO while remaining below the critical pH where Ce^{3+} precipitates as $Ce(OH)_3$ (solubility product constant $K_{sp} = 1.6 \times 10^{-20}$). This resulted in the formation of $Ce(OH)_x^+$ clusters, which were adsorbed onto the negatively charged CuO surface. Instead of aggregating, these clusters formed separated nano-islands due to electrostatic repulsion. The loading of CeO_x nano-islands could be controlled by adjusting the amount of KOH added. After calcination in air at 623 K, the CeO_x/CuO catalyst was successfully synthesized.

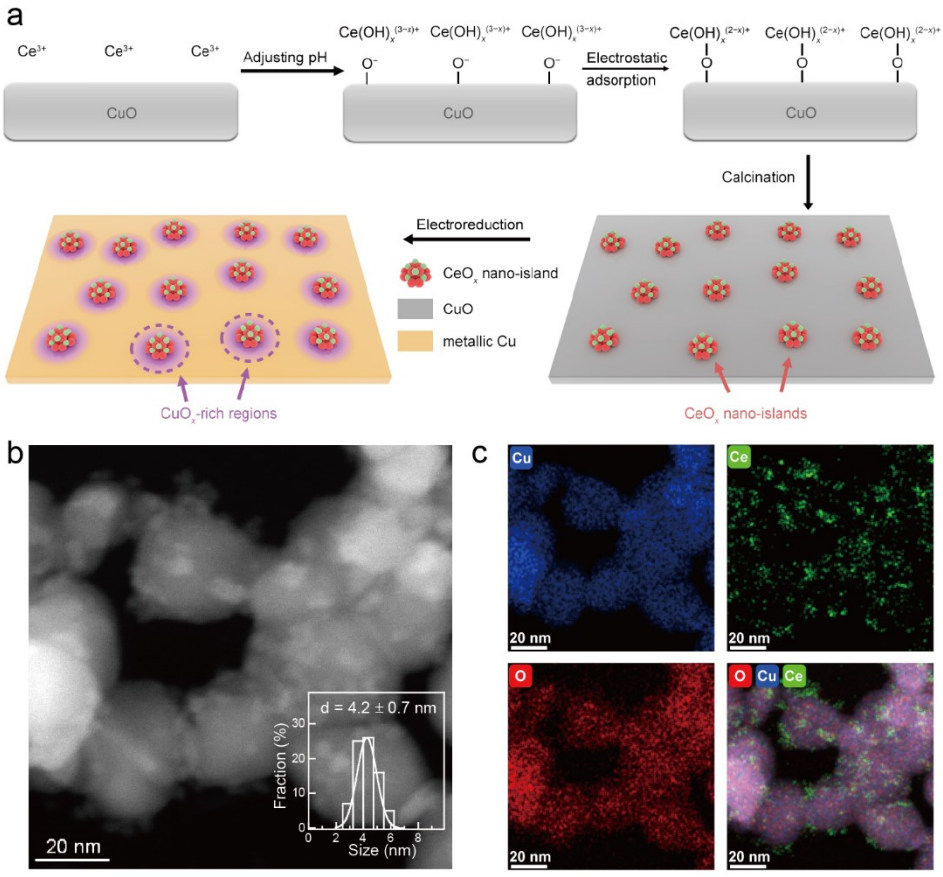

Figure 2 (a) Schematic illustration of the electrostatic absorption method and the CuO_x rich region introduced by CeO_2 nano-islands after *in-situ* electrochemical reduction. (b) HAADF-STEM image of CeO_x/CuO. (c) The corresponding EDS mappings.

We then characterized the as-synthesized catalysts using various techniques. Inductively

coupled plasma optical emission spectrometry (ICP-OES) analysis revealed a Ce/Cu mass ratio of 0.02 (Table S1). X-ray diffraction (XRD) patterns (Fig. S2) revealed predominant peaks for monoclinic CuO (space group C2/c) in both CeO_x/CuO and CuO, along with minor peaks for cubic CeO_2 (space group *Fm*-3*m*) in the CeO_x/CuO catalysts. High-angle annular dark-field scanning transmission electron microscopy (HAADF-STEM) images (Fig. 2b) revealed the presence of numerous nano-islands with an average diameter of 4.2 nm uniformly distributed on the CuO surface. These nano-islands exhibited a consistent morphology across a range of transmission electron microscopy (TEM) images (Fig. S3). Energy dispersive spectroscopy (EDS) elemental mapping (Fig. 2c) confirmed that the nano-islands consisted of Ce (green) and O (red). High-resolution transmission electron microscopy (HRTEM) images of CeO_x/CuO revealed distinct lattice fringes for CeO_2 and CuO, with spacings of 0.32 nm and 0.28 nm for the CeO_2 (111) and (200) planes, respectively, and 0.18 nm for the CuO (112) plane (Fig. S4). The Ce 3*d* X-ray photoelectron spectroscopy (XPS) revealed 26.1% Ce^{3+} species in CeO_x/CuO (x = 1.87, Fig. S5a), indicating the existence of oxygen vacancies in the ceria phase. The Cu *LM*2 Auger spectra of CeO_x/CuO suggested that Cu was predominantly in the oxidation state of +2 (Fig. S5b). These results confirmed the presence of approximately 4 nm CeO_x particles dispersed on CuO. To investigate the adaptability of the electrostatic adsorption method, we varied the Ce loading by adjusting the amount of KOH added during synthesis. As shown in Fig. S6, increasing the KOH beyond the optimal point (~2% Ce) did not lead to additional Ce incorporation onto the CuO surface. Instead, it resulted in the formation of discrete Ce-containing precipitates, indicating saturation of available adsorption sites. Conversely, reducing the Ce precursor led to catalysts with lower Ce loadings, which were systematically characterized by ICP-OES (Table S1), and electron microscopy (Fig. S7).

To evaluate the C–C coupling efficiencies of the CeO_x/CuO and CuO catalysts, the CO_2RR was conducted in a flow-cell configuration. Across all applied potentials, the CeO_x/CuO catalyst consistently exhibited a higher C_{2+} FE than CuO did (Fig. 3a and b; detailed product distribution in Fig. S8a and b, with error bars of at least four independent tests). Notably, the CeO_x/CuO catalyst achieved a maximum C_{2+} FE of 78% with a partial current density of −545 mA cm^{-2} at −1.6 V *vs*. RHE, with ethylene (C_2H_4) as the primary product (48% FE, Fig. S8a). In contrast, the CuO catalyst without CeO_x modification produced CO as the main product (Fig. S8b). As can be seen, the deposition of CeO_x on the CuO catalyst significantly enhanced both the C_{2+} FEs and

partial current densities of the C_{2+} products (Fig. 3a and b). To investigate whether the increased current density resulted from a greater active surface area, we measured the double-layer capacitance to determine the electrochemically active surface area (ECSA). Surprisingly, the ECSA of CeO_x/CuO was smaller than that of CuO (Fig. S9), despite the similar CuO morphologies of both catalysts. This reduction in the ECSA is likely due to the increased hydrophobicity introduced by surface modification with CeO_x nano-islands [44]. The water contact angle of CuO is 19.4° (Fig. S10a), while the contact angle increased to 66.6° after CeO_x nano-islands were introduced (Fig. S10b). Based on the ECSA measurements, the ECSA-normalized partial current density for the C_{2+} products was calculated against the applied potential for both catalysts (Fig. 3c). The results revealed significantly higher normalized C_{2+} current densities for CeO_x/CuO, confirming its superior intrinsic activity in the CO_2RR. We also conducted the CO_2RR under both acidic and alkaline conditions (Fig. S11). At a current density of −600 mA cm^{-2}, the CeO_x/CuO catalyst consistently exhibited over 70% C_{2+} FE, indicating that CeO_x nano-islands effectively promotes C_{2+} generation across diverse environments and also demonstrating the broad applicability of this catalyst.

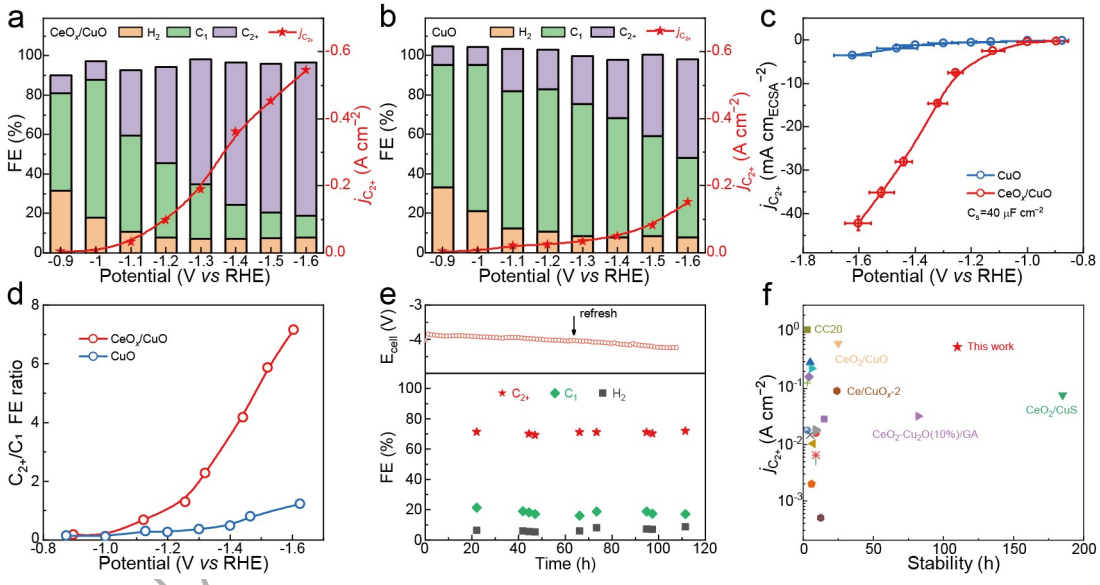

Figure 3 Distribution of products in the CO_2RR and partial current densities of the C_{2+} product at different potentials in a flow cell of the (a) CeO_x/CuO and (b) CuO catalysts. (c) Variation in the ESCA correlated partial current density of the C_{2+} product against the applied potential over CeO_x/CuO (red) and CuO (blue). (d) Ratio of C_{2+} to C_1 products at different potentials. (e) Duration test of CeO_x/CuO in an MEA reactor. (f) Comparison of the partial current densities of

C_{2+} products and long-term stabilities of CeO_x/CuO with those of other CuCe-based catalysts reported in the literature.

To further examine the C–C coupling efficiency, the C_{2+}/C_1 product FE ratio was calculated for both catalysts (Fig. 3d). Compared with the CuO catalyst, the CeO_x/CuO catalyst presented a significantly higher C_{2+}/C_1 ratio. At −1.4 V *vs*. RHE, the CeO_x/CuO catalyst had a C_{2+}/C_1 ratio of 4.2, which was 7 times greater than that of the CuO catalyst (a C_{2+}/C_1 ratio of 0.5). At −1.6 V *vs*. RHE, the C_{2+}/C_1 ratio of the CeO_x/CuO catalyst reached as high as 7.2, whereas that of the CuO catalyst remained at 1.2, indicating that CeO_x nano-islands modification enhanced the C–C coupling efficiency. The CeO_x/CuO catalyst also demonstrated high stability in the CO_2RR. In a flow cell configuration, the CeO_x/CuO catalyst exhibited >40% C_2H_4 FE at a high current density of −400 mA cm^{-2} for more than 15 hours (Fig. S12a). The performance dropped after 15 hours due to salt precipitate and flooding (Fig. S12b and c). To value the intrinsic stability of the CeO_x/CuO catalyst under industrially relevant conditions, duration test was also conducted in a membrane electrode assembly (MEA) configuration (Fig. 3e). the CeO_x/CuO catalyst maintained a C_{2+} FE exceeding 70% at a current density of −100 mA cm^{-2} for over 110 hours. Post-catalysis analysis confirmed the retention of the CeO_x structure. HRTEM images verified the dispersion of CeO_x nano-islands across the Cu surface (Fig. S13). The *quasi-in-situ* Ce 3*d* XPS spectra revealed 35.0% Ce^{3+} species on CeO_x/CuO (x = 1.83), which indicated that the CeO_x/CuO catalyst was stable because of its low solubility and reduced reducibility of CeO_x (Fig. S5c). XRD pattern of CeO_x/CuO after reaction showed a higher $Cu_2O(111)/Cu(111)$ peak ratio than that of CuO (Fig. S14). These results demonstrated the structural stability of the catalysts throughout the CO_2RR process. Compared with other CeCu-based catalysts reported in previous studies [29–31,34, 39–42,45–55] (Fig. 3f and Fig. S15), the CeO_x/CuO catalyst outperformed these materials, demonstrating both a high partial current density for C_{2+} products and robust stability. The improved performance was presumably attributed to the inertness of CeO_x and the hydrophobicity introduced by the nano-islands, which together enhance the stability and activity of the catalyst.Unexpectedly, the productivity of CO, a representative C_1 product, was not suppressed in the presence of CeO_x nano-islands, as demonstrated by *operando* differential electrochemical mass spectrometry (DEMS, Fig. 4a). Both the CeO_x/CuO and CuO catalysts exhibited similar onset potentials (−0.63 V *vs*. RHE) for CO production. However, the onset potential for C_2H_4 on CeO_x/CuO was −0.52 V *vs*. RHE, which is significantly more positive than

that on CuO (−0.65 V *vs*. RHE), indicating that the *CO coverage required for effective C–C coupling on CeO_x/CuO was lower. This observation suggested that the CeO_x nano-islands enhanced the C–C coupling process without inhibiting C_1 production.

To investigate the impact of CeO_x nano-islands on the electronic structure of Cu during the CO_2RR, *operando* X-ray absorption near edge structure (XANES) and extended X-ray absorption fine structure (EXAFS) analyses were performed. The first derivatives of the XANES data (Fig. 4b) revealed that CuO was quickly reduced to metallic Cu under negative potentials. In contrast, CeO_x/CuO exhibited features of both metallic Cu and Cu^{2+}, indicating partial reduction. The Cu^{2+} content decreased progressively with increasing negative potential, but did not fully disappear, suggesting that the CeO_x nano-islands effectively stabilized Cu^{2+}. The white line peaks of CeO_x/CuO (Fig. S16a) displayed characteristics of both Cu^{2+} and metallic Cu, whereas CuO (Fig. S16b) showed only metallic Cu features after reduction. These results highlight that CeO_x nano-islands impede the full reduction of Cu, preserving a fraction of Cu in its higher oxidation state. The EXAFS spectra further supported these findings. For CuO (Fig. 4c), the Cu–O bonds disappeared at modestly negative potentials, whereas the Cu–Cu bonds formed immediately upon the application of a negative potential, indicating that CuO was highly susceptible to reduction. In contrast, for CeO_x/CuO, the number of Cu–O bonds gradually decreased as the potential became more negative, persisting even under highly reductive conditions. Cu–Cu bonds only became dominant at −0.8 V *vs*. RHE or at more negative potentials, confirming that the presence of CeO_x nano-islands hindered the reduction of CuO.

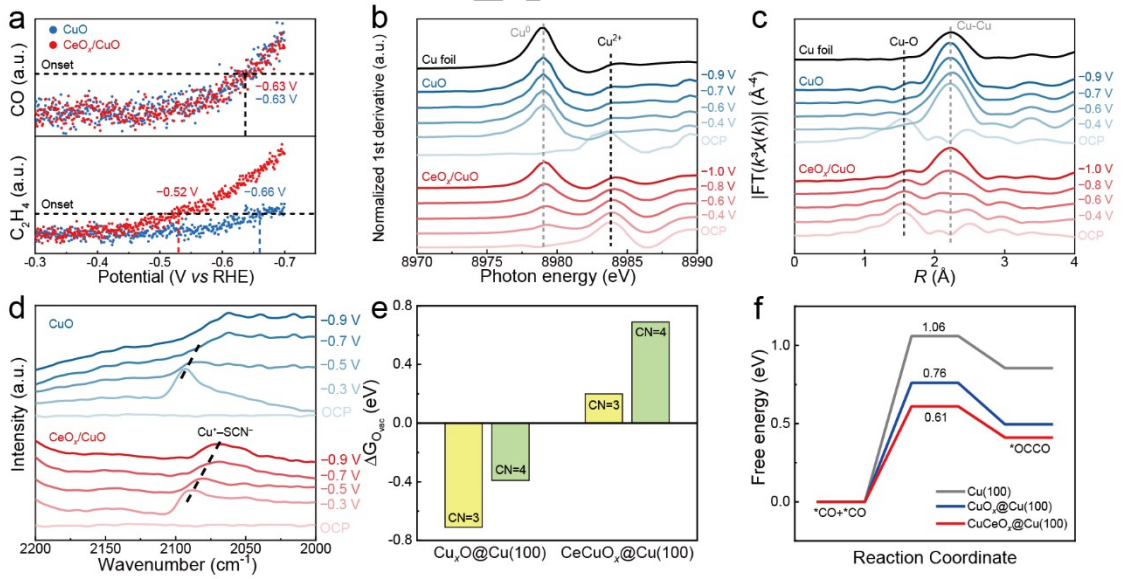

Figure 4 (a) *Operando* DEMS of CO and C_2H_4 during the CO_2RR on the CeO_x/CuO and CuO catalysts. (b) First derivatives of the *operando* Cu K-edge XANES spectra of CuO and CeO_x/CuO at different potentials. (c) *Operando* EXAFS spectra of the CuO and CeO_x/CuO catalysts at different potentials. (d) *Operando* ATR-SEIRAS of CuO and CeO_x/CuO in CO_2 purged 0.1 M $KHCO_3$ at different potentials, with 0.04 M KSCN used as a probe molecule for the generation of Cu^+ during electrolysis. (e) Oxygen vacancy formation energies of different coordination numbers on different surfaces. (f) Reaction barriers of *CO dimerization on various surfaces.

Operando Raman spectroscopy provided further evidence supporting the stabilizing effect of CeO_x nano-islands on Cu–O species (Fig. S17). Peaks at approximately 600 cm^{-1}, attributed to surface Cu–O species, disappeared on the CuO catalyst under negative potentials but remained detectable on the CeO_x/CuO catalyst, confirming the ability of CeO_x nano-islands to preserve surface Cu–O species under reducing conditions. Peaks at 800 cm^{-1} were attributed to peroxide vibration on CeO_x(111) [56]. This peak is absent in the CuO sample, confirming the successful deposition of CeO_x in the CeO_x/CuO composite. To directly probe the presence of surface Cu oxidized species on CeO_x/CuO, *operando* attenuated total reflection surface-enhanced infrared absorption spectroscopy (ATR-SEIRAS) was conducted using SCN^- as a probe molecule [57]. As shown in Fig. 4d, the peak at approximately 2073 cm^{-1} was attributed to Cu^+-SCN^- bonding. On the CuO surface, Cu^+ initially formed as the potential became negative, increasing in intensity before diminishing and disappearing below the detection limit at potentials more negative than −0.7 V *vs*. RHE. In contrast, on the CeO_x/CuO surface, the Cu^+-SCN^- peaks followed a similar trend of initial increase and subsequent decrease but remained detectable throughout the entire test. These results indicate that Cu^+ species formed on both catalysts; however, the Cu^+ on the CuO catalyst was more readily reduced to metallic Cu, whereas the Cu^+ on CeO_x/CuO was stabilized by the CeO_x nano-islands, persisting even under highly reductive conditions. Furthermore, the *quasi-in-situ* Cu *LM*2 Auger spectra of CeO_x/CuO after the duration test revealed a mixture of metallic Cu, Cu^+, and Cu^{2+} features (Fig. S5d), indicating that the higher oxidation state of Cu was stabilized by CeO_x. This highlights the critical role of CeO_x nano-islands in maintaining the active Cu^+ species, which are essential for efficient CO_2RR and enhanced C–C coupling.

Based on these characterizations, we propose a model in which CeO_x nano-islands create and stabilize CuO_x regions on the CeO_x/CuO catalyst during the CO_2RR (Fig. 2a, highlighted in

purple circles). The CeO_x nano-islands effectively modulate the electronic structure of Cu, allowing the retention of Cu in oxidized states under reducing conditions. These CuO_x regions serve as critical active sites, facilitating C–C coupling and thereby significantly enhancing the C_{2+} efficiency. In addition, the inert nature of CeO_x and the hydrophobicity introduced by the nano-islands also contributed to the stabilization of the catalyst system, enabling sustained performance during long-term tests. This combination of activity enhancement and stability improvement highlights the effectiveness of CeO_x nano-islands in optimizing the performance of the CeO_x/CuO catalyst.

To delve into the origin of CeO_x nano-islands enhancing C–C coupling activity on Cu, we further conducted theoretical calculations. We constructed Cu_6O_6 and $Ce_3Cu_3O_9$ clusters on Cu (100) to compare the differences in oxygen vacancy (O_v) formation energy and the energy barriers of CO dimerization among the Cu (100), CuO_x-Cu (100), and $CeCuO_x$-Cu (100) surfaces or interfaces. For CuO_x species on a Cu surface, the Cu–O–Cu structure readily forms oxygen vacancies, indicating that Cu is prone to reduction (Fig. 4e). The free energies for forming vacancies at oxygen sites coordinated by three Cu atoms (Fig. S18a, yellow circle) and four Cu atoms (Fig. S18a, green circle) are −0.71 eV and −0.39 eV, respectively. In contrast, introducing CeO_x clusters results in the formation of Ce–O–Cu structures, where oxygen atoms are less susceptible to reduction. The vacancy formation free energies at analogous sites are +0.20 eV (Fig. S18b, yellow circle) and +0.69 eV (Fig. S18b, green circle). This suggests that CeO_x clusters help retain more oxygen on the Cu surface, thereby increasing the surface Cu valence state, which, as previously discussed, promotes C–C coupling. We further investigated the mechanism by which CuO_x species enhance C–C coupling. In the copper-based CO_2RR, multiple intermediates are involved in C–C coupling. To explore this process, we selected *CO dimerization as a model to compare the CeO_x/CuO catalyst with metallic Cu. On the Cu (100) surface, the coupling of bridge-adsorbed *CO + *CO involves four Cu atoms (Fig. S19a) and requires a high activation energy of 1.06 eV (Fig. 4f), indicating that C–C coupling is challenging on a metallic Cu surface. However, in the presence of CuO_x, the oxidized Cu stabilizes the *OC–CO intermediate through interactions with the oxygen atom in *CO (Fig. S19b), lowering the activation energy to 0.76 eV (Fig. 4f). Furthermore, Ce^{3+} ions in CeO_x clusters also stabilize the *OC–CO intermediate (Fig. S19c), further reducing the energy barrier for *CO + *CO coupling to 0.61 eV on the $CeCuO_x$@Cu (100) surface (Fig. 4f). This significant

reduction in the energy barrier demonstrated that CeO_x nano-islands and CuO_x species synergistically facilitated C–C coupling. These findings explain how the synergistic interaction between CeO_x nano-islands and CuO_x species enhances C–C coupling activity during the CO_2RR. The Ce–O–Cu structures at the CeO_x-CuO_x interface enhance the oxygen stability and maintain higher Cu valence states, whereas the stabilization of *OC–CO intermediates by CeO_x and CuO_x promotes efficient C_{2+} product formation in the CO_2RR.

Enhancing the FE of the target product holds significant importance for reducing the cost of electrochemical production. We analyzed the differences between CeO_x/CuO and CuO catalysts for ethylene production from these three perspectives (Fig. S20, Supplementary Note 1). Following the substitution of CuO with CeO_x/CuO for ethylene generation: carbon capture costs decreased by 70.2%, electrolysis energy costs decreased by 29.2%, and ethylene separation costs decreased by 62.7%. These results demonstrate the promising potential of the CeO_x/CuO catalyst for industrial application.

In summary, we demonstrated an effective strategy for constructing CeO_x nano-islands on Cu particles to promote C–C coupling efficiency in the CO_2RR. *Operando* XAFS and ATR-SEIRAS combined with *quasi-in-situ* XPS revealed that CeO_x nano-islands effectively stabilize Cu^+ and Cu^{2+} species under reductive conditions, preserving the active oxidation states necessary for sustained catalytic performance. The catalyst achieved a remarkable FE of 78% for C_{2+} products at −700 mA cm^{-2}, with durability maintaining over 70% FE at −100 mA cm^{-2} for more than 110 hours. Theoretical calculations revealed that CeO_x promotes CuO_x formation, which is crucial for C_{2+}production, lowering the energy barrier for C–C coupling by stabilizing *OC–CO intermediates. This study underscores the dual role of CeO_x as both a stabilizer of CuO_x and a promoter of C_{2+} production. Importantly, this study highlights the potential for further optimization of activity, selectivity, and stability by exploring alternative elements as modifiers, paving the way for scalable and economically viable CO_2RR technologies

DATA AVAILABILITY

All data are available in the main text or the supplementary information.

ACKNOWLEDGMENTS

This work was partially carried out at the Instruments Center for Physical Science, University of Science and Technology of China.

FUNDING

This work was supported by the National Key Research and Development Program of China (2021YFA1500500), the CAS Project for Young Scientists in Basic Research (YSBR-051), the National Natural Science Foundation of China (22322201, 22278067, 22525021, 22221003, 22250007, 22361162655 and 22303093), the Science and Technology Development Fund (FDCT) of Macao S.A.R (0070/2023/AFJ), the Fundamental Research Funds for the Central Universities, the Joint Fund of the Yulin University and the Dalian National Laboratory for Clean Energy (YLU-DNL Fund 2022012), the State Key Laboratory of Catalysis (2024SKL-A-011), the International Partnership Program of Chinese Academy of Sciences (123GJHZ2022101GC), the Natural Science Foundation of Sichuan Province (2025NSFJQ0017), the Key Science & Technology Project of Anhui Province (202423110050009) and the Fundamental Research Funds for the Central Universities (ZYGX2022J012). J.Z. acknowledges support from the New Cornerstone Science Foundation through the XPLORER PRIZE.

AUTHOR CONTRIBUTIONS

M.W, T.Z. and J.Z. designed the study. M.W., J.L., Y.J., W.X., Y.D., H.W., X.Z, K.N.H and X.L. conducted the experiments. S.H. conducted HAADF-STEM analysis. J.Z. carried out DFT calculations. M.W., C.X., T.Z. and J.Z. wrote the paper. All authors discussed the results and contributed to the manuscript.

Conflict of interest statement. None declared.

REFERENCES

1. Hepburn C, Adlen E, Beddington J *et al*. The technological and economic prospects for CO_2

utilization and removal. *Nature* 2019; **575**: 87−97.

2. De Luna P, Hahn C, Higgins D *et al*. What would it take for renewably powered electrosynthesis to displace petrochemical processes? *Science* 2019; **364**: eaav3506.
3. Dinh C-T, Burdyny T, Kibria MG *et al*. CO_2 electroreduction to ethylene via hydroxide-mediated copper catalysis at an abrupt interface. *Science* 2018; **360**: 783−7.
4. Ding J, Yang HB, Ma X-L *et al*. A tin-based tandem electrocatalyst for CO_2 reduction to ethanol with 80% selectivity. *Nat Energy* 2023; **8**: 1386−94.
5. Yuan L-J, Sui X-L, Pan H *et al*. Strategies and mechanism for enhancing intrinsic activity of metal–nitrogen–carbon catalysts in electrocatalytic reactions. *Renewables* 2023; **1**: 514-540.
6. Gao D, Arán-Ais RM, Jeon HS *et al*. Rational catalyst and electrolyte design for CO_2 electroreduction towards multicarbon products. *Nat Catal* 2019; **2**: 198−210.
7. Wang Y, Liu J and Zheng G. Designing copper-based catalysts for efficient carbon dioxide electroreduction. *Adv Mater* 2021; **33**: e2005798.
8. Li J, Chang X, Zhang H *et al*. Electrokinetic and in situ spectroscopic investigations of CO electrochemical reduction on copper. *Nat Commun* 2021; **12**: 3264.
9. Deng W, Zhang P, Qiao Y *et al*. Unraveling the rate-determining step of C_{2+} products during electrochemical CO reduction. *Nat Commun* 2024; **15**: 892.
10. Zhan C, Dattila F, Rettenmaier C *et al*. Key intermediates and Cu active sites for CO_2 electroreduction to ethylene and ethanol. *Nat Energy* 2024; **9**: 1485−96.
11. Bian L, Bai Y, Chen J-Y *et al*. Hierarchical tandem catalysis promotes co spillover and trapping for efficient CO_2 reduction to C_{2+} products. *ACS Nano* 2025; **19**: 9304-9316
12. Chen L, Chen J, Fu W *et al*. Energy-efficient $CO_{(2)}$ conversion to multicarbon products at high rates on CuGa bimetallic catalyst. *Nat Commun* 2024; **15**: 7053
13. Zhao Y, Liu X, Chen J *et al*. Promote electroreduction of CO_2 via catalyst valence state manipulation by surface-capping ligand. *Proc Natl Acad Sci U.S.A* 2023; **120**: e2218040120
14. Fu W, Li Y, Chen J *et al*. Preserving molecular tuning for enhanced electrocatalytic CO_2-to-ethanol conversion. *Angew Chem Int Ed* 2024; **136**: e202407992
15. Li H, Jiang Y, Li X *et al*. C_{2+} selectivity for CO_2 electroreduction on oxidized Cu-based catalysts. *J Am Chem Soc* 2023; **145**: 14335−44.
16. Wu H, Huang L, Timoshenko J *et al*. Selective and energy-efficient electrosynthesis of ethylene from CO_2 by tuning the valence of Cu catalysts through aryl diazonium

functionalization. *Nat Energy* 2024; **9**: 422−33.

17. Herzog A, Luna ML, Jeon HS *et al*. Operando Raman spectroscopy uncovers hydroxide and CO species enhance ethanol selectivity during pulsed CO_2 electroreduction. *Nat Commun* 2024; **15**: 3986.
18. Lin S-C, Chang C–C, Chiu S-Y *et al*. Operando time-resolved X-ray absorption spectroscopy reveals the chemical nature enabling highly selective CO_2 reduction. *Nat Commun* 2020; **11**: 3525.
19. Yang H, Li S and Xu Q. Efficient strategies for promoting the electrochemical reduction of CO_2 to C_{2+} products over Cu-based catalysts. *Chin J Catal* 2023; **48**: 32−65.
20. Timoshenko J, Bergmann A, Rettenmaier C *et al*. Steering the structure and selectivity of CO_2 electroreduction catalysts by potential pulses. *Nat Catal* 2022; **5**: 259−67.
21. Cao Y, Chen Z, Li P *et al*. Surface hydroxide promotes CO_2 electrolysis to ethylene in acidic conditions. *Nat Commun* 2023; **14**: 2387.
22. Liu H, Yang C, Bian T *et al*. Bottom-up growth of convex sphere with adjustable Cu(0)/Cu(I) interfaces for effective C_2 production from CO_2 electroreduction. *Angew Chem Int Ed* 2024; **63**: e202404123.
23. Yang Y, Louisia S, Yu S *et al*. Operando studies reveal active Cu nanograins for CO_2 electroreduction. *Nature* 2023; **614**: 262−9.
24. Lian Z, Dattila F and López N. Stability and lifetime of diffusion-trapped oxygen in oxide-derived copper CO_2 reduction electrocatalysts. *Nat Catal* 2024; **7**: 401−11.
25. Choi W, Chae Y, Liu E *et al*. Exploring the influence of cell configurations on Cu catalyst reconstruction during CO_2 electroreduction. *Nat Commun* 2024; **15**: 8345.
26. Feng J, Wu L, Liu S *et al*. Improving CO_2-to-C_{2+} product electroreduction efficiency via atomic Lanthanide dopant-induced tensile-strained CuO_x catalysts. *J Am Chem Soc* 2023; **145**: 9857−66.
27. Du Y-R, Li X-Q, Duan G-Y *et al*. Sn-based redox cycle mediated microenvironment regulation of Cu sites on poly(ionic liquid) enhance electrocatalytic CO-to-C_{2+} conversion. *Appl Catal B* 2023; **337**: 122969.
28. Zhang XY, Lou ZX, Chen J *et al*. Direct OC–CHO coupling towards highly C_{2+} products selective electroreduction over stable Cu^0/Cu^{2+} interface. *Nat Commun* 2023; **14**: 7681.
29. Zhao Z, Li X, Wang J *et al*. CeO_2-modified Cu electrode for efficient CO_2 electroreduction

to multi-carbon products. *J CO2 Util* 2021; **54**: 101741.

30. Wang H, Zhang H, Huang Y *et al*. Strain in copper/ceria heterostructure promotes electrosynthesis of multicarbon products. *ACS Nano* 2023; **17**: 346−54.
31. Yang Z, Ji D, Li Z *et al*. CeO_2/CuS nanoplates electroreduce CO_2 to ethanol with stabilized Cu^+ species. *Small* 2023; **19**: e2303099.
32. Tian H, Yang J-T, Wang X *et al*. Ionic liquid-TiO_2-CuO_x composite interfaces combined with gas directional transmission for enhanced electrooxidation of methane to ethanol. *Appl Catal B-Environ* 2025; **375**: 125411
33. Tian H, Zhang Z-Y, Fang H *et al*. Selective electrooxidation of methane to formic acid by atomically dispersed CuO_x and its induced Lewis acid sites on V_2O_5 in a tubular electrode. *Appl Catal B-Environ* 2024; **351**: 124001
34. Hong S, Abbas HG, Jang K *et al*. Tuning the C_1/C_2 selectivity of electrochemical CO_2 reduction on Cu-CeO_2 nanorods by oxidation state control. *Adv Mater* 2023; **35**: e2208996.
35. Sultan S, Lee H, Park S *et al*. Interface rich CuO/Al_2CuO_4 surface for selective ethylene production from electrochemical CO_2 conversion. *Energy Environ Sci* 2022; **15**: 2397−409.
36. Hu X, Xu J, Gao Y *et al*. Establishing non-stoichiometric Ti_4O_7 assisted asymmetrical C–C coupling for highly energy-efficient electroreduction of carbon monoxide. *Angew Chem Int Ed* 2024; **64**: e202414416.
37. Chang C-J, Lai Y-A, Chu Y-C *et al*. Lewis acidic support boosts C–C coupling in the pulsed electrochemical CO_2 reaction. *J Am Chem Soc* 2023; **145**: 6953−65.
38. Kou T, Wang S, Yang S *et al*. Amorphous CeO_2-Cu heterostructure enhances CO_2 electroreduction to multicarbon alcohols. *ACS Materials Lett* 2022; **4**: 1999−2008.
39. Sun Y, Xie J, Fu Z *et al*. Boosting CO_2 electroreduction to C_2H_4 via unconventional hybridization: high-order Ce^{4+} 4f and O 2p interaction in Ce-Cu_2O for stabilizing Cu^+. *ACS Nano* 2023; **17**: 13974−84.
40. Luo M, Wang Z, Li YC *et al*. Hydroxide promotes carbon dioxide electroreduction to ethanol on copper via tuning of adsorbed hydrogen. *Nat Commun* 2019; **10**: 5814.
41. Varandili SB, Huang J, Oveisi E *et al*. Synthesis of Cu/CeO_{2-x} nanocrystalline heterodimers with interfacial active sites to promote CO_2 electroreduction. *ACS Catal* 2019; **9**: 5035−46.
42. Yan X, Chen C, Wu Y *et al*. Efficient electroreduction of CO_2 to C_{2+} products on CeO_2 modified CuO. *Chem Sci* 2021; **12**: 6638−45.

43. Li X, Pereira-Hernandez XI, Chen Y *et al*. Functional CeO_x nanoglues for robust atomically dispersed catalysts. *Nature* 2022; **611**: 284−8.
44. Azimi G, Dhiman R, Kwon HM *et al*. Hydrophobicity of rare-earth oxide ceramics. *Nat Mater* 2013; **12**: 315−20.
45. Wu D, Dong C, Wu D *et al*. Cuprous ions embedded in ceria lattice for selective and stable electrochemical reduction of carbon dioxide to ethylene. *J Mater Chem A* 2018; **6**: 9373−7.
46. Yin J, Gao Z, Wei F *et al*. Customizable CO_2 electroreduction to C_1 or C_{2+} products through Cu_y/CeO_2 interface engineering. *ACS Catal* 2022; **12**: 1004−11.
47. Shan J, Shi Y, Li H *et al*. Effective CO_2 electroreduction toward C_2H_4 boosted by Ce-doped Cu nanoparticles. *Chem Eng J* 2022; **433**: 133769.
48. Chu M, Chen C, Wu Y *et al*. Enhanced CO_2 electroreduction to ethylene via strong metal-support interaction. *Green Energy Environ* 2022; **7**: 792−8.
49. Tian Y, Fei X, Ning H *et al*. Membrane-free electrocatalysis of CO_2 to C_2 on CuO/CeO_2 nanocomposites. *Front Chem* 2022; **10**: 915759.
50. Yap FM, Loh JY, Yuan S *et al*. Revolutionizing CO_2-to-C_2 conversion: unleashing the potential of CeO_2 nanocores for self-supported electrocatalysts with Cu_2O nanoflakes on 3D graphene aerogel. *Adv Funct Mater* 2025; **35**: 2407605.
51. Chu S, Yan X, Choi C *et al*. Stabilization of Cu^+ by tuning a $CuO\text{-}CeO_2$ interface for selective electrochemical CO_2 reduction to ethylene. *Green Chem* 2020; **22**: 6540−6.
52. Tan D, Wulan B, Cao X *et al*. Strong interactions of metal-support for efficient reduction of carbon dioxide into ethylene. *Nano Energy* 2021; **89**: 106460.
53. Cai H-D, Nie B, Guan P *et al*. Tuning the interactions in CuO nanosheet-decorated CeO_2 nanorods for controlling the electrochemical reduction of CO_2 to methane or ethylene. *ACS Appl Nano Mater* 2022; **5**: 7259−67.
54. Liu X, Liu T, Ouyang T *et al*. Ce^{3+}/Ce^{4+} Ion redox shuttle stabilized $Cu^{\delta+}$ for efficient CO_2 electroreduction to C_2H_4. *Angew Chem Int Ed* 2024, **64**: e202419796.
55. Qiao Y, Shen S, Mao C *et al*. Interfacial oxygen vacancy-copper pair sites on inverse CeO_2/Cu catalyst enable efficient CO_2 electroreduction to ethanol in acid. *Angew Chem Int Ed* 2025; **64**: e202424248.
56. Schilling C, Hofmann A, Hess C *et al*. Raman spectra of polycrystalline CeO_2: a density functional theory study. *J Phys Chem C* 2017; **121**: 20834–20849.

57. Wu J, Xu L, Kong Z *et al*. Integrated tandem electrochemical-chemical-electrochemical coupling of biomass and nitrate to sustainable alanine. *Angew Chem Int Ed* 2023; **62**: e202311196.